Frontiers of Information Technology & Electronic Engineering
www.jzus.zju.edu.cn; engineering.cae.cn; www.springerlink.com
ISSN 2095-9184 (print); ISSN 2095-9230 (online)
E-mail: jzus@zju.edu.cn

# Passive mode-locked Er-doped fiber laser pulse generation based on titanium disulfide saturable absorber*

Xinxin SHANG[1,3,4], Linguang GUO[1,3,4], Huanian ZHANG[†2], Dengwang LI[1,3,4], Qingyang YUE[†‡1,3,4]

[1]*Shandong Provincial Engineering and Technical Center of Light Manipulations, Shandong Provincial Key Laboratory of Optics and Photonic Device, School of Physics and Electronics, Shandong Normal University, Jinan 250358, China*

[2]*School of Physics and Optoelectronic Engineering, Shandong University of Technology, Zibo 255049, China*

[3]*Shandong Key Laboratory of Medical Physics and Image Processing, School of Physics and Electronics, Shandong Normal University, Jinan 250358, China*

[4]*Shandong Institute of Industrial Technology for Health Sciences and Precision Medicine, School of Physics and Electronics, Shandong Normal University, Jinan 250358, China*

[†]E-mail: huanian_zhang@163.com; qingyangyue@sdnu.edu.cn

Received July 11, 2020; Revision accepted Aug. 10, 2020; Crosschecked Mar. 29, 2021; Published online Mar. 31, 2021

**Abstract:** In this study, titanium disulfide ($TiS_2$) polyvinyl alcohol (PVA) film-type saturable absorber (SA) is synthesized with a modulation depth of 5.08% and a saturable intensity of 10.62 MW/cm$^2$ by liquid-phase exfoliation and spin-coating methods. Since $TiS_2$-based SA has a strong nonlinear saturable absorption property, two types of optical soliton were observed in a mode-locked Er-doped fiber laser. When the pump power was raised to 67.3 mW, a conventional mode-locked pulse train with a repetition rate of 1.716 MHz and a pulse width of 6.57 ps was generated, and the output spectrum centered at 1556.98 nm and 0.466 nm spectral width with obvious Kelly sidebands was obtained. Another type of mode-locked pulse train with the maximum output power of 3.92 mW and pulse energy of 2.28 nJ at the pump power of 517.2 mW was achieved when the polarization controllers were adjusted. Since $TiS_2$-based SA has excellent nonlinear saturable absorption characteristics, broad applications in ultrafast photonic are expected.

**Key words:** Fiber laser; Passive mode-locked; Saturable absorber; Titanium disulfide
https://doi.org/10.1631/FITEE.2000341 **CLC number:** TN244

## 1 Introduction

Over the past decade, ultrafast fiber lasers have attracted great attention due to their low price, compact structure, and high environmental stability, which have made them widely applied in biomedicine, spectroscopy, imaging, material processing, and other fields (Keller, 2003; Shah et al., 2006; Oktem et al., 2010; Sheng et al., 2013; Cai et al., 2018; Guo LG et al., 2019). In 1985, ultrashort pulse chirped amplification technology played a significant role in removing a huge hurdle in further increasing the laser intensity under mode-locked technology. This in turn helped ultrafast lasers enter a new era of development and application. Passive mode-locked and Q-switched techniques are commonly used and effective methods for generating ultrashort pulsed lasers. Most of fiber lasers use the passive mode-locked technique to achieve ultrashort pulse operation, adopted by a nonlinear optical modulator, named the saturable

‡ Corresponding author

* Project supported by the National Natural Science Foundation of China (Nos. 11904213 and 11747149), the Shandong Provincial Natural Science Foundation (Nos. ZR2018QF006 and ZR2019MF029), the China Postdoctoral Science Foundation (No. 2016M602177), and the Opening Foundation of Shandong Provincial Key Laboratory of Laser Technology and Application

ORCID: Xinxin SHANG, https://orcid.org/0000-0003-0611-014X; Qingyang YUE, https://orcid.org/0000-0002-1241-8469

absorber (SA), which converts continuous wave output into a series of optical pulses. It was acknowledged that graphene plays a key role in exploring new two-dimensional (2D) SAs. In addition, possessing ultrafast carrier dynamics and high third-order nonlinear susceptibility has made graphene widely used in photonic devices including SAs, optical modulators, and optical switches (Bao et al., 2009; Hendry et al., 2010). Afterwards, several other types of graphene-like 2D materials such as black phosphorous, topological insulators (TIs), MXene, and transition metal dichalcogenides (TMDs) were used as SAs (Zhang HN and Liu, 2016; Guo B, 2018; Jiang et al., 2018; Ming et al., 2018; Niu et al., 2018; Guo B et al., 2019; Guo SY et al., 2019; Hu et al., 2019; Liu JS et al., 2019; Song et al., 2019; Xu NN et al., 2019, 2020; Xu YJ et al., 2019; Zhao et al., 2019; Li L et al., 2020a, 2020b; Liu WJ et al., 2020a, 2020b; Zhang HN et al., 2020). The discovery of new SA materials with ultrafast recovery, high damage threshold, and wide absorption band has always been in a desired condition.

In recent years, monolayer and multilayer TMDs such as molybdenum disulfide ($MoS_2$), molybdenum diselenide ($MoSe_2$), tungsten disulfide ($WS_2$), tungsten diselenide ($WSe_2$), and tin disulfide ($SnS_2$) have been extensively studied and employed as SAs. TMDs are known as 2D materials because of their excellent photoelectronic applications. TMDs' properties such as remarkably large third-order nonlinear susceptibility (Niu et al., 2017), abundance of transition metal d electrons (Friend and Yoffe, 1987; Butler et al., 2013; Xu XD et al., 2014; Yan et al., 2017), layer structure, and semi-conductive capabilities with thickness-dependent band gap could support broadband saturable absorption (Mak et al., 2010; Ciarrocchi et al., 2018). $TiS_2$ is a typical TMD material with multilayer structure, made up of a Ti layer sandwiched between two S layers in an octahedral configuration (Fang et al., 1997), and has the potential for exfoliation from the bulk to ultrathin multilayers due to the weak van der Walls force between layers (Park et al., 2008; Zeng et al., 2011, 2012). It has been successfully adopted in many applications, such as photoelectrochemical hydrogen generation (Dolui and Sanvito, 2016), battery electrodes (Zhang XQ et al., 2018), and photodetectors (Zhu ZF et al., 2016). An apparent overlap of the valence and conduction bands proves that $TiS_2$ has a vast tunable band gap from about 0.05 eV for bulk structure to about 2.87 eV for 1–3 layer structures (Li TY et al., 2014; Dolui and Sanvito, 2016; Varma et al., 2017; Ge et al., 2018), which in turn facilitates converting a wide spectral region range from visible to infrared (Ge et al., 2018; Zhu X et al., 2018). Other 2D materials, such as SnS, SnSe, and Se in IV–VI group and VI element, have proved to generate laser pulse as SAs (Xing et al., 2017; Wu et al., 2018; Xie et al., 2019). Xing et al. (2017) discovered the saturable absorption of Se and generated mode-locked pulse of 3.1 ps centered at 1555.67 nm. The modulation depth of the Se SA was 2.13%. An all-optical switching technique based on multilayer SnS was proposed through modulating the propagation of the signal beam by another controlling beam due to its large Kerr nonlinearity. Xie et al. (2019) reported both Q-switched and mode-locked operations based on SnS. The SAs were prepared using the liquid-phase exfoliation method with a modulation depth of 36.4% and a saturable intensity of 34.8 GW/cm$^2$. It is of great significance to explore the nonlinear optical absorption properties of $TiS_2$ and apply $TiS_2$ in various fields.

In this study, an Er-doped fiber laser based on a $TiS_2$-PVA nanosheet is reported as an SA with obvious polarization-dependent saturable absorption. Both traditional mode-locked pulses and high pulse energy mode-locked pulses were obtained, and nonlinear optical properties of $TiS_2$-PVA nanosheets were investigated experimentally. Results showed that the saturation intensity and modulation depth were about 10.62 MW/cm$^2$ and 5.08%, respectively. The traditional mode-locked pulse centered at 1556.98 nm with a 3 dB bandwidth of 0.466 nm with obvious Kelly sidebands. When the pump power increased to 67.3 mW, the pulse width was 6.57 ps with a fundamental repetition rate of 1.716 MHz. In addition, high pulse energy mode-locked pulse was observed when we adjusted the polarization controllers. Further, stable mode-locked state was maintained when the pump power increased from 77.4 mW to 517.2 mW. The maximum output power was 3.92 mW corresponding to the highest single pulse energy of 2.28 nJ. Our experimental results proved that $TiS_2$ can be an excellent SA in a fiber laser.

## 2 Preparation, characterization, and optical properties of TMD:$TiS_2$-PVA nanosheets

In recent work, different composite polymers were employed to be combined with 2D nanomaterials such as polyvinyl alcohol (PVA), polystyrene (PS), and polyvinylpyrrolidone (PVP) (Ge et al., 2019; Guo J et al., 2019). In this study, PVA composite polymers were employed because of their advantages, such as low cost, simple preparation, and good stability. In addition, PVA composite polymers have no effect on the nonlinearity in the cavity. Single- or multi-layer of 2D materials can be obtained using different methods (Ding et al., 2015; Hao et al., 2016; Huang et al., 2018, 2019, 2020). Liquid-phase exfoliation technology was adopted to obtain $TiS_2$ nanosheets. The $TiS_2$-PVA film used in our experiment was fabricated by homogenously mixing $TiS_2$ solution into PVA solution and spin coating in culture dish. First, $TiS_2$ solution was prepared by adding 0.5 g of $TiS_2$ powder into 50 mL of alcohol (30%). The solution was transferred into an ultrasonic cleaner for 8 h for producing multi-layer $TiS_2$ nanosheets. We added 2 g PVA into 50 mL distilled (DI) water. Then, it was consistently stirred using a magnetic stirrer for about 12 h at a constant speed of 2000 r/min. Afterwards, the $TiS_2$ solution was gently poured into the prepared PVA solution at a volume ratio of 1:1 and placed in the ultrasonic cleaner for 8 h for preparing uniform $TiS_2$-PVA solution. The homogenously dispersed $TiS_2$-PVA solution was then spin-coated into a clean culture dish. To form a semi-transparent $TiS_2$-PVA film, the solution was left to dry and evaporate at room temperature for 12 h. Finally, a piece of film with the size of about 1 mm×1 mm was gently cut off and attached on a clean FC/PC fiber ferrule as a proposed modulator.

The surface morphology of samples was characterized by scanning electron microscopy (SEM) (Sigma 500, ZEISS). Fig. 1a shows the SEM image of $TiS_2$ powder. An obvious layered structure can be

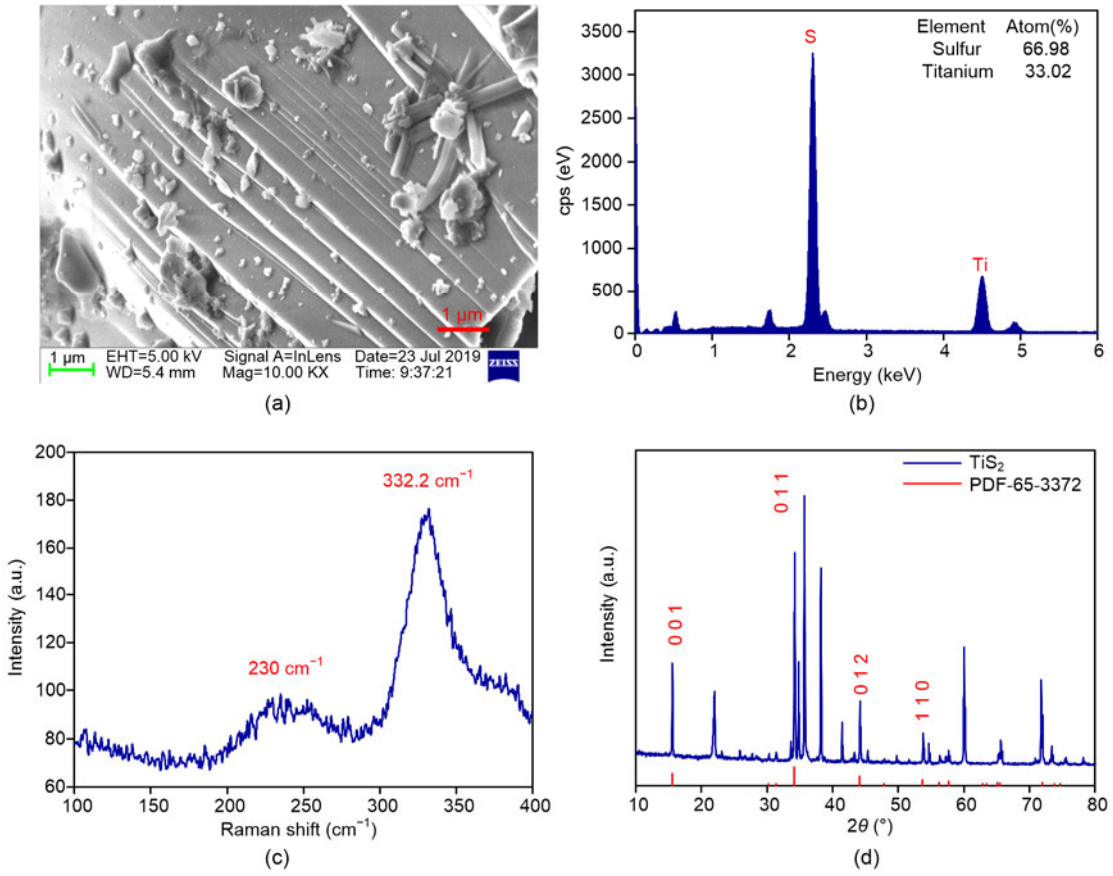


**Fig. 1 Scanning electron microscopy (SEM) image of $TiS_2$ powder (a), energy dispersion X-ray spectroscopy (EDS) spectrum of $TiS_2$ powder (b), Raman spectrum of $TiS_2$ powder excited by a 532-nm laser (c), and X-ray diffraction (XRD) analysis for $TiS_2$ powder (d) (References to color refer to the online version of this figure)**

observed in the diagram, which indicates that the nanosheets can be exfoliated through the liquid-phase exfoliation method. In addition, the size of nanoparticles was nonuniform because it had not stripped from the bulk $TiS_2$. Fig. 1b presents the corresponding energy dispersion X-ray spectroscopy (EDS) (XFlash 6130, Bruker) spectrum of the $TiS_2$ powder. The peaks associated with titanium and sulfide were clearly observed. The structure and quality of the experimental sample were tested by a Raman spectrometer (Horiba HR Evolution 800) and X-ray diffraction (XRD) (D8 Advance Bruker). The Raman spectrum was measured at 532-nm-excitation wavelength at room temperature (Fig. 1c). The Raman spectrum with two Raman shift peaks at 332.2 $cm^{-1}$ and 230 $cm^{-1}$, which corresponded to $A_{1g}$ (polarization of vibration of S ions along the c-axis) and $E_g$ (polarization of vibration of S in-plane normal to the c-axis) modes respectively, were observed (Sandoval et al., 1992; Zhang X et al., 2016; Suri et al., 2017). As provided by XRD in Fig. 1d, main diffraction peaks located at 001, 011, 012, and 110, which is consistent with the $TiS_2$ crystal spectrum in the standard spectrum library (PDF-65-3372).

Fig. 2a demonstrates that $TiS_2$ nanosheets were obtained after liquid-phase dissection. The transmission electron microscope (TEM) image of the $TiS_2$ nanosheets dispersion solution was detected by a JEM-2100 microscope with an optical resolution of 200 nm for testing the layered structure properties of $TiS_2$ dispersion. Fig. 2b shows the corresponding selected-area electron diffraction. The results indicated that the $TiS_2$ nanosheets prepared in our experiment have a layered structure with high crystallinity. The thickness of the $TiS_2$ nanosheets was characterized by an atomic force microscope (AFM) (Bruker Multimode 8). The AFM image was depicted in Fig. 2c. The obvious layered structure can be observed combined with AFM test, which proved that the material was successfully dissected and that

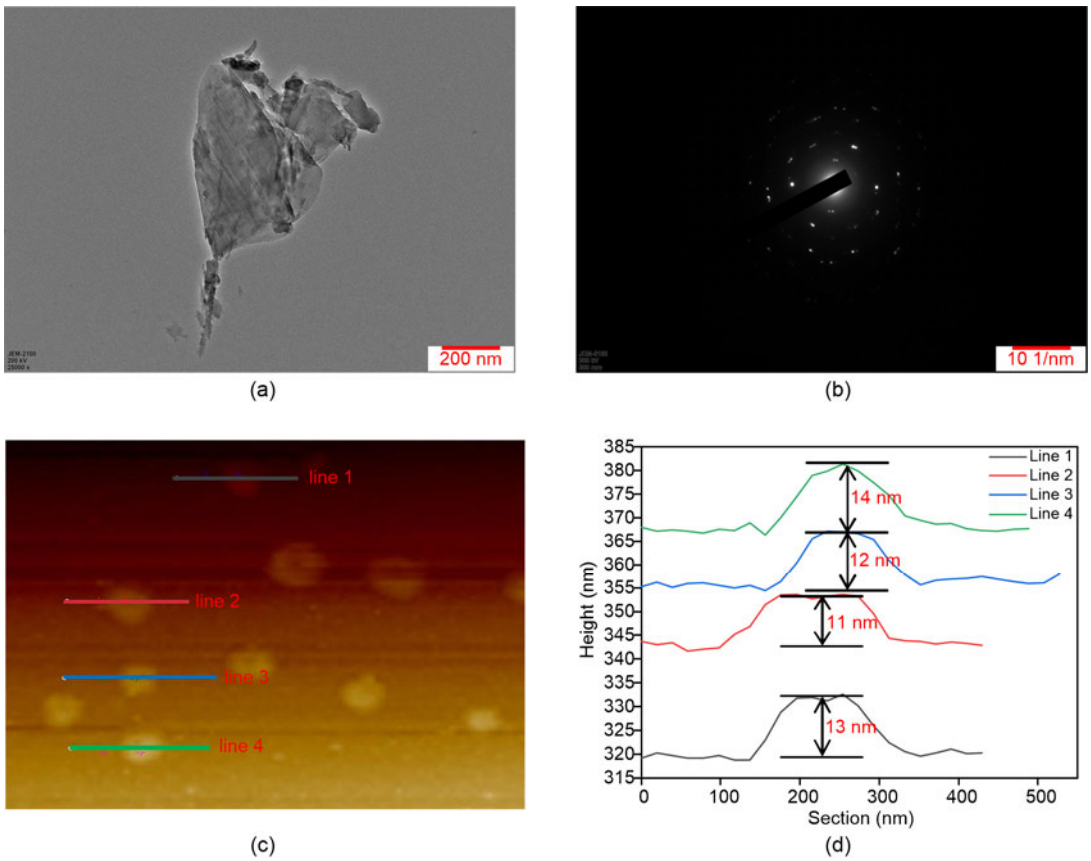


**Fig. 2 Transmission electron microscope (TEM) image of $TiS_2$ nanosheets (a), selected-area electron diffraction (b), atomic force microscope (AFM) image of $TiS_2$ nanosheets (c), and the corresponding measurement of height of the selected area in Fig. 2c (d) (References to color refer to the online version of this figure)**

thinner $TiS_2$ nanosheets were obtained. Fig. 2d shows that the corresponding heights were about 11, 12, 13, and 14 nm. Fig. 2c shows the AFM image of $TiS_2$ nanosheets corresponding to the atomic layer numbers of about 19–25, where the monolayer thickness of $TiS_2$ was 0.57 nm (Lin et al., 2013). Therefore, layered $TiS_2$ nanosheets were stripped successfully.

The linear optical transmission spectrum of the $TiS_2$-PVA film was measured by a UV/vis/NIR spectrophotometer (Hitachi U-4100, Tokyo, Japan) and displayed in Fig. 3a. The transmittance coefficient increased along with the wavelength from 900 to 1800 nm. The transmission of the $TiS_2$-PVA film at the wavelength of 1557 nm was about 81%. A power-dependent transmission technique was employed to measure the nonlinear absorption properties of the $TiS_2$-PVA film-type SA. In our experiment, $TiS_2$ SA exhibited an excellent saturable absorption property, as shown in Fig. 3b. Based on the well-known formula explained in Gao et al. (2019), the fitting curve showed that the saturation intensity and modulation depth were 10.62 MW/cm$^2$ and 5.08%, respectively.

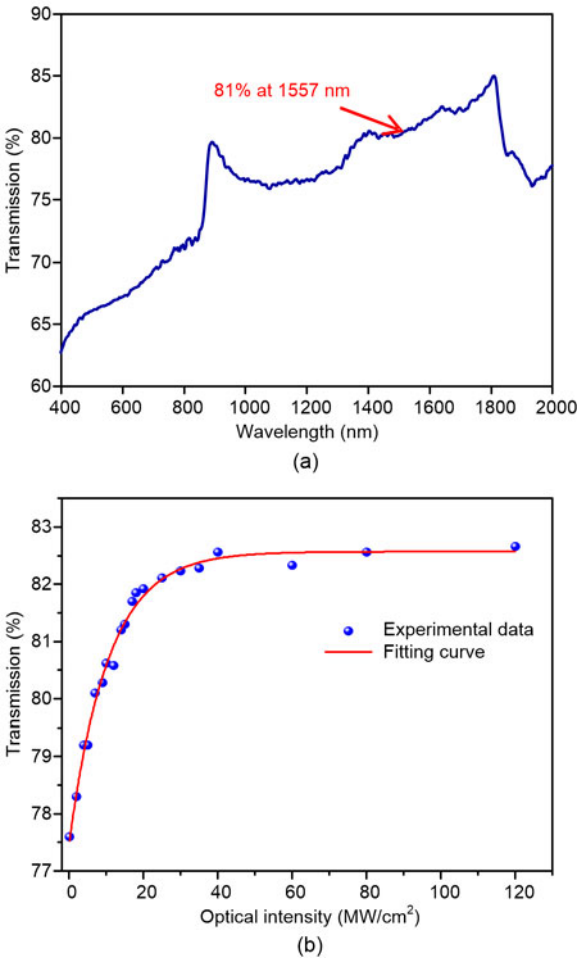


**Fig. 3 Linear transmission of the $TiS_2$-PVA film (a) and nonlinear absorption curve of $TiS_2$-PVA SA (b)**

## 3 Experimental setup

The schematic of passive mode-locked Er-dope fiber laser is shown in Fig. 4. A 119.7-m-long ring cavity design was adopted, including 31.7-cm long Er-doped fiber (Er-110) with an absorption of 110 dB/m at 1530 nm. A dispersion value of about −46 ps/(nm·km) at 1550 nm was used as gain medium and 119.4-m-long single-mode fiber with dispersion parameter of about 17 ps/(nm·km) was added into the cavity. The net dispersion of the Er-doped fiber laser was calculated to be −2.75 ps$^2$. The pumping signal was introduced by a 980 nm laser source with the highest pump power of 517.2 mW through a 980/1550 nm wavelength division multiplexer. A polarization-independent isolator (PI-ISO), to ensure unidirectional propagation, and a PC were employed to adjust the net birefringence. A 10% output coupler was used to direct the output signal. Furthermore, the output characteristics were analyzed by a 3-GHz photo detector combined with a digital oscilloscope (Tektronix DPO 4054, USA) and another digital oscilloscope (Wavesurfer 3054, Teledyne LeCroy, USA), a radio frequency spectrum (R&S FPC1000, Jena, Germany), an optical spectrum analyzer (AQ6317B, Yokogawa, Tokyo, Japan), a power meter (PM100D-S122C, Thorlabs, New Jersey, USA), and an intensity autocorrelator (Femtochrome FR-103XL, USA).

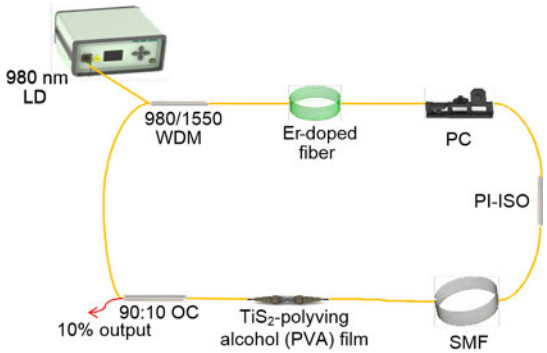


**Fig. 4 Schematic of passive mode-locked fiber laser**

## 4 Results and discussion

We measured the operation characteristics of the laser without $TiS_2$-PVA film before carrying out the experiment. There was only continuous wave output no matter how the pump power and polarization states of PC were adjusted, which excludes the possibility of the mode-locked operation due to the nonlinear polarization rotation and the Fabry–Perot cavity effect. Fig. 5c depicts the pulse train beyond $TiS_2$-PVA film was added into the cavity, as shown in Fig. 4. The stable traditional mode-locked pulse can be obtained by increasing the pump power from 67 mW to 192 mW and rotating the PC with extra care. The output characteristics of the stable mode-locked operation under the pump power of 192 mW are depicted in Fig. 5. Fig. 5a shows the typical soliton-like spectrum shape with obvious Kelly sidebands at a resolution of 0.02 nm. The central wavelength and 3 dB bandwidth were 1556.98 nm and 0.466 nm, respectively. The relationship between the average output power and pump powers is shown in Fig. 5b. The output power and pump power showed a linear correlation. Under the pump power of 192 mW, the output power was 0.87 mW, which corresponded to an optical conversion efficiency of 0.45%. Fig. 5c depicts the pulse train beyond the mode-locked operation. The pulse-to-pulse time was 582.9 ns, which matched well the round-trip time of the cavity. The single profile of the pulse was characterized using an intensity autocorrelator (Fig. 5d). The plot fitted well with a Gaussian shape pulse with a duration of 6.57 ps (deconvolved). The time-bandwidth product was calculated to be about 0.379, near the theoretical limit value of 0.315.

To test the stability of the $TiS_2$-PVA based mode-locked laser, we measured its radio frequency (RF) spectrum. The fundamental peak located at the repetition rate of 1.716 MHz with a signal-to-noise ratio of about 55 dB (Fig. 6a). The RF spectrum within a wide bandwidth of 100 MHz with the resolution of 3 kHz is shown in Fig. 6b for investigating the long-term

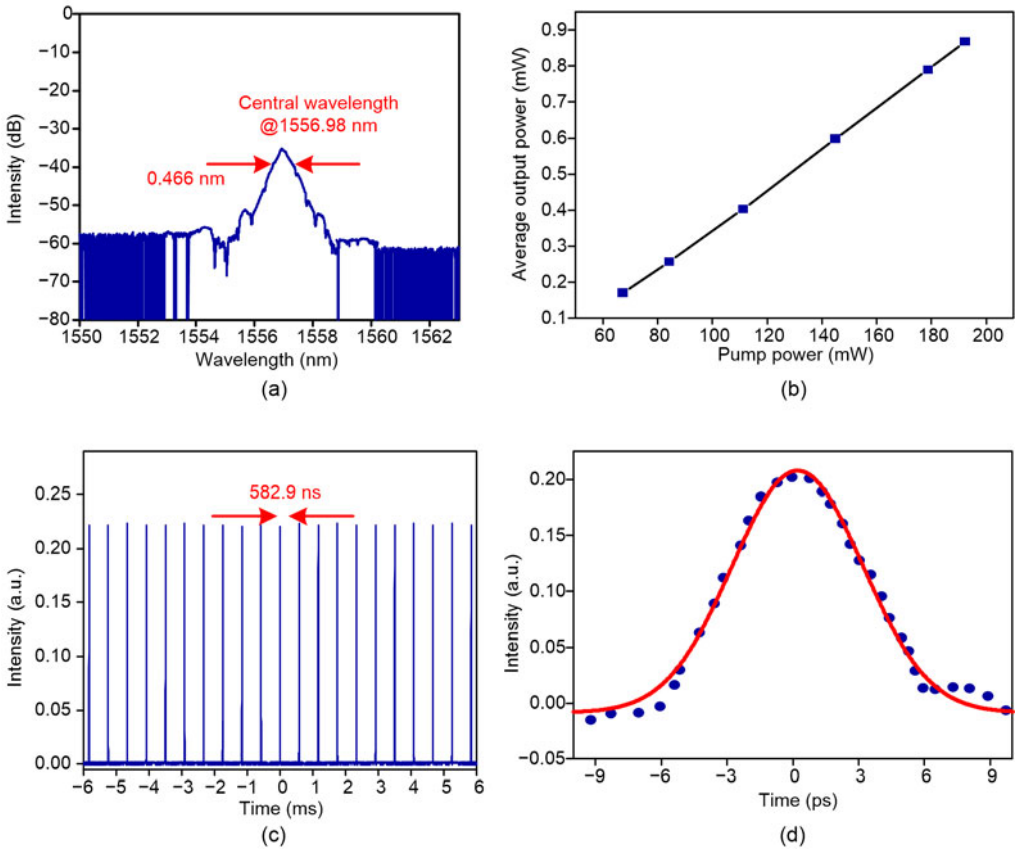


**Fig. 5 Typical optical spectrum with obvious Kelly sidebands (a), the relationship between pump power and average output power (b), output mode-locked pulse train (c), and measured autocorrelation trace and its fitted curve (d)**

stability of the laser. The experimental results indicated that the stable soliton pulse operation was achieved successfully. We also measured the stability of the optical spectrum with the change of pump power and time. Fig. 6c presents the relationship between the optical spectrum and different pump power. Their central spectral peak locations were intact, but the spectral width was broadened with the increase of pump power. We continuously monitored the evolution of optical spectra at intervals of 30 min over 3 h to evaluate the long-term stability of the fiber laser. As sketched in Fig. 6d, the Kelly sidebands of the spectrum did not change with time. Their central wavelength, spectral bandwidth, and spectral intensity were reasonably stable over the time. All the results exhibited that traditional mode-locked pulses with high stability were obtained in this study.

Another mode-locked pulse with high pulse energy was obtained when we adjusted the PC. Fig. 7a demonstrates the optical spectrum of the soliton pulse with increasing the pump power from 77.4 mW to 517.2 mW. Further increasing the pump power did not make significant change in the optical spectrum and waveform. There were two stable wavelengths located near 1557 nm. Figs. 7c and 7d present the pulse train and the corresponding single pulse profile, respectively. The time interval for pulse train was 582.9 ns, which corresponded to the fundamental repetition rate of 1.716 MHz. Fig. 7b displays the average output power and pulse energy performance as a function of pump power. The threshold pump power of the mode-locked fiber laser was 77.4 mW. The average output power and pulse energy increased almost linearly in correspondence to the increase of pump power. Notably, the output power was 3.92 mW under the maximum pump power of 517.2 mW, which corresponded to an optical-to-optical conversion efficiency of 0.76%. Higher output power can provide

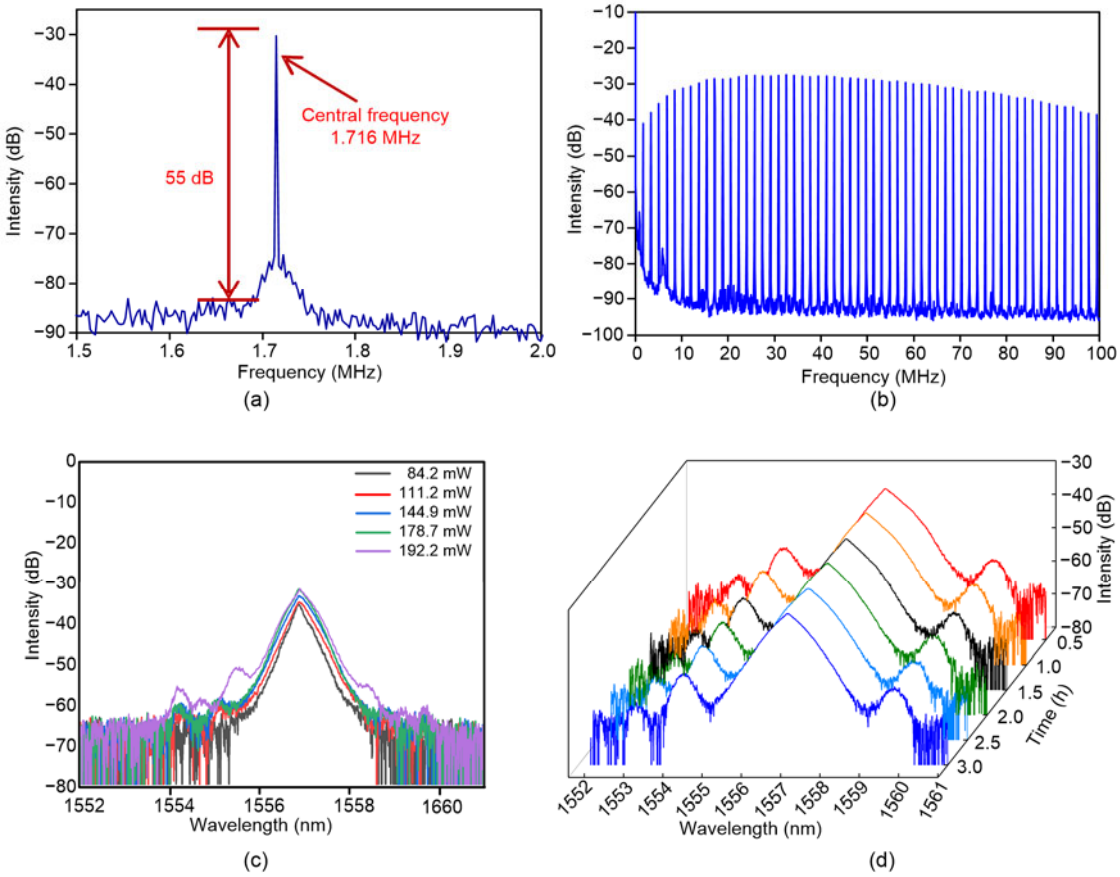


**Fig. 6 Radio frequency (RF) spectrum at the fundamental frequency of 1.716 MHz (a), the higher harmonics on a span of 100 MHz (b), the change of the optical spectrum under different pump powers (c), and long-term stability: optical spectra measured at a 0.5 h interval over 3 h (d) (References to color refer to the online version of this figure)**

more sufficient power security for other versatile applications such as mid-IR fiber sensor/communication, medical diagnosis, and materials processing. The maximum single pulse energy achieved was as high as about 2.28 nJ, which proved that $TiS_2$-PVA nanosheets have a high optical damage threshold.

We also measured the fundamental RF spectrum to investigate the stability of the laser. Fig. 8a presents the signal-to-noise ratio of the RF spectrum, which was >70 dB, implying low-amplitude fluctuation and good mode-locking stability. To verify the stability of this operation, a wideband RF spectrum up to 20 MHz is presented in Fig. 8b. No extra spectrum was

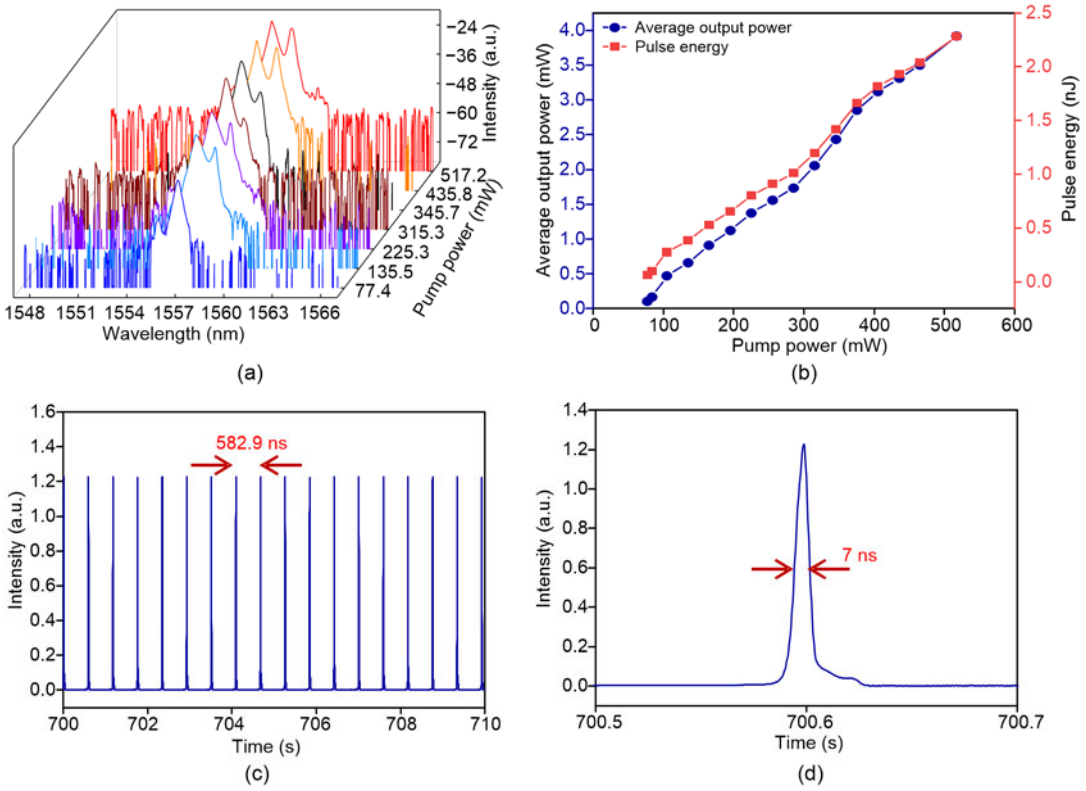


**Fig. 7 Change of the optical spectrum under different pump powers (a), average output power and pulse energy performances with the increase of pump power (b), the pulse train at the mode-locked operation (c), and the corresponding single pulse profile (d)**

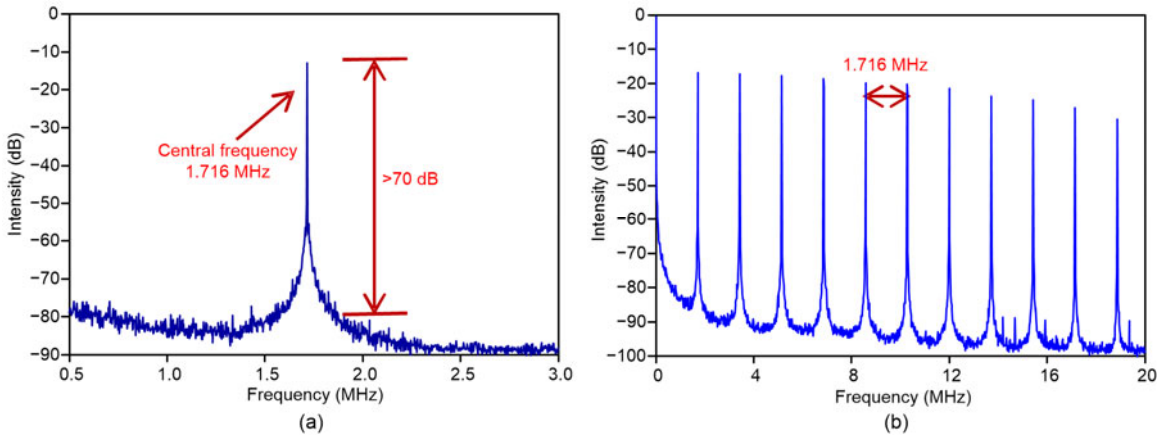


**Fig. 8 The fundamental RF spectrum of the laser output (a) and the wideband RF spectrum up to 20 MHz (b)**

observed, indicating that stable mode-locked operation was obtained.

## 5 Conclusions

The strong saturable absorption of $TiS_2$-PVA SA was demonstrated employing the liquid-phase exfoliation and spin-coating methods. The results showed that $TiS_2$-PVA nanosheets display an ultrafast nonlinear saturable absorption property and high optical damage threshold. The saturation intensity and modulation depth of $TiS_2$-PVA nanosheets were 10.62 MW/cm$^2$ and 5.08%, respectively. We obtained both traditional mode-locked pulse and high pulse energy mode-locked pulse in an Er-doped fiber laser based on the $TiS_2$-PVA nanosheet. The conventional mode-locked pulse with a pulse width of 6.57 ps centered at 1556.98 nm and another mode-locked pulse with the highest single pulse energy of 2.28 nJ were obtained. Experimental results revealed that $TiS_2$ nanosheets are promising ultrafast nonlinear optical materials for applications in mid-IR mode-locked fiber laser.

### Contributors

Xinxin SHANG designed the research and drafted the manuscript. Linguang GUO helped organize the manuscript. Huanian ZHANG processed the data. Dengwang LI and Qingyang YUE collected the relevant materials. Xinxin SHANG revised and finalized the paper.

### Compliance with ethics guidelines

Xinxin SHANG, Linguang GUO, Huanian ZHANG, Dengwang LI, and Qingyang YUE declare that they have no conflict of interest.

### References

Bao QL, Zhang H, Wang Y, et al., 2009. Atomic-layer graphene as a saturable absorber for ultrafast pulsed lasers. *Adv Funct Mater*, 19(19):3077-3083. https://doi.org/10.1002/adfm.200901007

Butler SZ, Hollen SM, Cao LY, et al., 2013. Progress, challenges, and opportunities in two-dimensional materials beyond graphene. *ACS Nano*, 7(4):2898-2926. https://doi.org/10.1021/nn400280c

Cai JH, Chen H, Chen SP, et al., 2018. Compressibility of dissipative solitons in mode-locked all-normal-dispersion fiber lasers. *J Lightw Technol*, 36(11):2142-2151. https://doi.org/10.1109/JLT.2018.2806226

Ciarrocchi A, Avsar A, Ovchinnikov D, et al., 2018. Thickness-modulated metal-to-semiconductor transformation in a transition metal dichalcogenide. *Nat Commun*, 9(1):919. https://doi.org/10.1038/s41467-018-03436-0

Ding SN, Jin Y, Chen X, et al., 2015. Tunable electrochemiluminescence of CdSe@ZnSe quantum dots by adjusting ZnSe shell thickness. *Electrochem Commun*, 55:30-33. https://doi.org/10.1016/j.elecom.2015.03.011

Dolui K, Sanvito S, 2016. Dimensionality-driven phonon softening and incipient charge density wave instability in $TiS_2$. *Europhys Lett*, 115(4):47001. https://doi.org/10.1209/0295-5075/115/47001

Fang CM, de Groot RA, Haas C, 1997. Bulk and surface electronic structure of 1 T-$TiS_2$ and 1 T-$TiSe_2$. *Phys Rev B*, 56(8):4455-4463. https://doi.org/10.1103/PhysRevB.56.4455

Friend RH, Yoffe AD, 1987. Electronic properties of intercalation complexes of the transition metal dichalcogenides. *Adv Phys*, 36(1):1-94. https://doi.org/10.1080/00018738700101951

Gao JJ, Zhou Y, Liu YJ, et al., 2019. Noise-like mode-locked Yb-doped fiber laser in a linear cavity based on $SnS_2$ nanosheets as a saturable absorber. *Appl Opt*, 58(22): 6007-6011. https://doi.org/10.1364/AO.58.006007

Ge YQ, Zhu ZF, Xu YH, et al., 2018. Broadband nonlinear photoresponse of 2D $TiS_2$ for ultrashort pulse generation and all-optical thresholding devices. *Adv Opt Mater*, 6(4):1701166. https://doi.org/10.1002/adom.201701166

Ge YQ, Huang WC, Yang FM, et al., 2019. Beta-lead oxide quantum dot (β-PbO QD)/polystyrene (PS) composite films and their applications in ultrafast photonics. *Nanoscale*, 11(14):6828-6837. https://doi.org/10.1039/C9NR01112A

Guo B, 2018. 2D noncarbon materials-based nonlinear optical devices for ultrafast photonics. *Chin Opt Lett*, 16(2): 020004. https://doi.org/10.3788/COL201816.020004

Guo B, Xiao QL, Wang SH, et al., 2019. 2D layered materials: synthesis, nonlinear optical properties, and device applications. *Laser Photon Rev*, 13(12):1800327. https://doi.org/10.1002/lpor.201800327

Guo J, Zhao JL, Huang DZ, et al., 2019. Two-dimensional tellurium–polymer membrane for ultrafast photonics. *Nanoscale*, 11(13):6235-6242. https://doi.org/10.1039/C9NR00736A

Guo LG, Shang XX, Zhao R, et al., 2019. Nonlinear optical properties of ferromagnetic insulator $Cr_2Ge_2Te_6$ and its application for demonstrating pulsed fiber laser. *Appl Phys Expr*, 12(8):082006. https://doi.org/10.7567/1882-0786/ab2dcc

Guo SY, Zhang YP, Ge YQ, et al., 2019. 2D V-V binary materials: status and challenges. *Adv Mater*, 31(39):1902352. https://doi.org/10.1002/adma.201902352

Hao C, Shen, YR, Wang, ZY, et al., 2016. Preparation and characterization of $Fe_2O_3$ nanoparticles by solid-phase method and its hydrogen peroxide sensing properties. *ACS Sustain Chem Eng*, 4(3):1069-1077. https://doi.org/10.1021/acssuschemeng.5b01150

Hendry E, Hale PJ, Moger J, et al., 2010. Coherent nonlinear optical response of graphene. *Phys Rev Lett*, 105(9): 097401. https://doi.org/10.1103/PhysRevLett.105.097401

Hu QY, Zhang XY, Liu ZJ, et al., 2019. High-order harmonic mode-locked Yb-doped fiber laser based on a $SnSe_2$ saturable absorber. *Opt Laser Technol*, 119:105639. https://doi.org/10.1016/j.optlastec.2019.105639

Huang WC, Xing CY, Wang YZ, et al., 2018. Facile fabrication and characterization of two-dimensional bismuth(III) sulfide nanosheets for high-performance photodetector applications under ambient conditions. *Nanoscale*, 10(5):2404-2412. https://doi.org/10.1039/C7NR09046C

Huang WC, Zhang Y, You Q, et al., 2019. Enhanced photodetection properties of Tellurium@Selenium roll-to-roll nanotube heterojunctions. *Small*, 15(23):1900902. https://doi.org/10.1002/smll.201900902

Huang WC, Li C, Gao LF, et al., 2020. Emerging black phosphorus analogue nanomaterials for high-performance device applications. *J Mater Chem C*, 8(4):1172-1197. https://doi.org/10.1039/C9TC05558D

Jiang XT, Zhang LJ, Liu SX, et al., 2018. Ultrathin metal–organic framework: an emerging broadband nonlinear optical material for ultrafast photonics. *Adv Opt Mater*, 6(16):1800561. https://doi.org/10.1002/adom.201800561

Keller U, 2003. Recent developments in compact ultrafast lasers. *Nature*, 424(6950):831-838. https://doi.org/10.1038/nature01938

Li L, Pang LH, Zhao QY, et al., 2020a. Niobium disulfide as a new saturable absorber for an ultrafast fiber laser. *Nanoscale*, 12(7):4537-4543. https://doi.org/10.1039/C9NR10873D

Li L, Pang LH, Zhao QY, et al., 2020b. $VSe_2$ nanosheets for ultrafast fiber lasers. *J Mater Chem C*, 8(3):1104-1109. https://doi.org/10.1039/C9TC06159B

Li TY, Liu YH, Chitara B, et al., 2014. Li intercalation into 1D $TiS_2$(en) chains. *J Am Chem Soc*, 136(8):2986-2989. https://doi.org/10.1021/ja4132399

Lin CW, Zhu XJ, Feng J, et al., 2013. Hydrogen-incorporated $TiS_2$ ultrathin nanosheets with ultrahigh conductivity for stamp-transferrable electrodes. *J Am Chem Soc*, 135(13): 5144-5151. https://doi.org/10.1021/ja400041f

Liu JS, Li XH, Guo YX, et al., 2019. $SnSe_2$ nanosheets for subpicosecond harmonic mode-locked pulse generation. *Small*, 15(38):1902811. https://doi.org/10.1002/smll.201902811

Liu WJ, Liu ML, Liu XM, et al., 2020a. Recent advances of 2D materials in nonlinear photonics and fiber lasers. *Adv Opt Mater*, 8(8):1901631. https://doi.org/10.1002/adom.201901631

Liu WJ, Liu ML, Liu XM, et al., 2020b. SnSSe as a saturable absorber for an ultrafast laser with superior stability. *Opt Lett*, 45(2):419-422. https://doi.org/10.1364/OL.380183

Mak KF, Lee C, Hone J, et al., 2010. Atomically thin $MoS_2$: a new direct-gap semiconductor. *Phys Rev Lett*, 105(13): 136805. https://doi.org/10.1103/PhysRevLett.105.136805

Ming N, Tao SN, Yang WQ, et al., 2018. Mode-locked Er-doped fiber laser based on PbS/CdS core/shell quantum dots as saturable absorber. *Opt Expr*, 26(7): 9017-9026. https://doi.org/10.1364/OE.26.009017

Niu KD, Chen QY, Sun RY, et al., 2017. Passively Q-switched erbium-doped fiber laser based on $SnS_2$ saturable absorber. *Opt Mater Expr*, 7(11):3934-3943. https://doi.org/10.1364/OME.7.003934

Niu KD, Sun RY, Chen QY, et al., 2018. Passively mode-locked Er-doped fiber laser based on $SnS_2$ nanosheets as a saturable absorber. *Photon Res*, 6(2):72-76. https://doi.org/10.1364/PRJ.6.000072

Oktem B, Ülgüdür C, Ilday FÖ, 2010. Soliton–similariton fibre laser. *Nat Photon*, 4(5):307-311. https://doi.org/10.1038/nphoton.2010.33

Park KH, Choi J, Kim HJ, et al., 2008. Unstable single-layered colloidal $TiS_2$ nanodisks. *Small*, 4(7):945-950. https://doi.org/10.1002/smll.200700804

Sandoval SJ, Chen XK, Irwin JC, 1992. Raman spectra of $Ag_xTiS_2$ and lattice dynamics of $TiS_2$. *Phys Rev B*, 45(24):14347-14353. https://doi.org/10.1103/PhysRevB.45.14347

Shah L, Fermann ME, Dawson JW, et al., 2006. Micromachining with a 50 W, 50 μJ, sub-picosecond fiber laser system. *Opt Expr*, 14(25):12546-12551. https://doi.org/10.1364/OE.14.012546

Sheng QW, Feng M, Xin W, et al., 2013. Actively manipulation of operation states in passively pulsed fiber lasers by using graphene saturable absorber on microfiber. *Opt Expr*, 21(12):14859-14866. https://doi.org/10.1364/OE.21.014859

Song YF, Shi XJ, Wu CF, et al., 2019. Recent progress of study on optical solitons in fiber lasers. *Appl Phys Rev*, 6(2):021313. https://doi.org/10.1063/1.5091811

Suri D, Siva V, Joshi S, et al., 2017. A study of electron and thermal transport in layered titanium disulphide single crystals. *J Phys Conden Mat*, 29(48):485708. https://doi.org/10.1088/1361-648X/aa90c5

Varma SJ, Kumar J, Liu Y, et al., 2017. 2D $TiS_2$ layers: a superior nonlinear optical limiting material. *Adv Opt Mater*, 5(24):1700713. https://doi.org/10.1002/adom.201700713

Wu LM, Xie ZJ, Lu L, et al., 2018. Few-layer tin sulfide: a promising black-phosphorus-analogue 2D material with exceptionally large nonlinear optical response, high stability, and applications in all-optical switching and wavelength conversion. *Adv Opt Mater*, 6(2):1700985. https://doi.org/10.1002/adom.201700985

Xie ZJ, Zhang F, Liang ZM, et al., 2019. Revealing of the ultrafast third-order nonlinear optical response and enabled photonic application in two-dimensional tin sulfide. *Photon Res*, 7(5):494-502. https://doi.org/10.1364/PRJ.7.000494

Xing CY, Xie ZJ, Liang ZM, et al., 2017. 2D nonlayered selenium nanosheets: facile synthesis, photoluminescence, and ultrafast photonics. *Adv Opt Mater*, 5(24):1700884. https://doi.org/10.1002/adom.201700884

Xu NN, Ming N, Han XL, et al., 2019. Large-energy passively Q-switched Er-doped fiber laser based on CVD-$Bi_2Se_3$ as saturable absorber. *Opt Mater Expr*, 9(2):373-383. https://doi.org/10.1364/OME.9.000373

Xu NN, Ma PF, Fu SG, et al., 2020. Tellurene-based saturable absorber to demonstrate large-energy dissipative soliton and noise-like pulse generations. *Nanophotonics*, 9(9): 2783-2795. https://doi.org/10.1515/nanoph-2019-0545

Xu XD, Liu W, Kim Y, et al., 2014. Nanostructured transition metal sulfides for lithium ion batteries: progress and challenges. *Nano Today*, 9(5):604-630. https://doi.org/10.1016/j.nantod.2014.09.005

Xu YJ, Shi Z, Shi XY, et al., 2019. Recent progress in black phosphorus and black-phosphorus-analogue materials: properties, synthesis and applications. *Nanoscale*, 11(31): 14491-14527. https://doi.org/10.1039/C9NR04348A

Yan PG, Chen H, Yin JD, et al., 2017. Large-area tungsten disulfide for ultrafast photonics. *Nanoscale*, 9(5):1871-1877. https://doi.org/10.1039/C6NR09183K

Zeng ZY, Yin ZY, Huang X, et al., 2011. Single-layer semiconducting nanosheets: high-yield preparation and device fabrication. *Angew Chem*, 123(47):11289-11293. https://doi.org/10.1002/ange.201106004

Zeng ZY, Sun T, Zhu JX, et al., 2012. An effective method for the fabrication of few-layer-thick inorganic nanosheets. *Angew Chem Int*, 51(36):9052-9056. https://doi.org/10.1002/anie.201204208

Zhang HN, Liu J, 2016. Gold nanobipyramids as saturable absorbers for passively Q-switched laser generation in the 1.1 μm region. *Opt Lett*, 41(6):1150-1152. https://doi.org/10.1364/OL.41.001150

Zhang HN, Ma PF, Zhu MX, et al., 2020. Palladium selenide as a broadband saturable absorber for ultra-fast photonics. *Nanophotonics*, 9(8):2557-2567. https://doi.org/10.1515/nanoph-2020-0116

Zhang X, Tan QH, Wu JB, et al., 2016. Review on the Raman spectroscopy of different types of layered materials. *Nanoscale*, 8(12):6435-6450. https://doi.org/10.1039/C5NR07205K

Zhang XQ, Zhong Y, Xia XH, et al., 2018. Metal-embedded porous graphitic carbon fibers fabricated from bamboo sticks as a novel cathode for lithium–sulfur batteries. *ACS Appl Mater Interf*, 10(16):13598-13605. https://doi.org/10.1021/acsami.8b02504

Zhao Y, Guo PL, Li XH, et al., 2019. Ultrafast photonics application of graphdiyne in the optical communication region. *Carbon*, 149:336-341. https://doi.org/10.1016/j.carbon.2019.04.075

Zhu X, Chen S, Zhang M, et al., 2018. $TiS_2$-based saturable absorber for ultrafast fiber lasers. *Photon Res*, 6(10): C44-C48. https://doi.org/10.1364/PRJ.6.000C44

Zhu ZF, Zou YS, Hu WD, et al., 2016. Near-infrared plasmonic 2D semimetals for applications in communication and biology. *Adv Funct Mater*, 26(11):1793-1802. https://doi.org/10.1002/adfm.201504884